CAMBRIDGE JOURNALS

Proof Delivery Form

Proceedings of the International Astronomical Union

Date of delivery: 5 May 2016

Journal and vol/article ref: | IAU | | 1600632 |

Number of pages (not including this page): 22

This proof is sent to you on behalf of Cambridge University Press. Please check the proofs carefully. Make any corrections necessary on a hardcopy and answer queries on each page of the proofs

Please return the **marked proof** within | **5** | days of receipt to:

Managing editor of this symposium

Authors are strongly advised to read these proofs thoroughly because any errors missed may appear in the final published paper. This will be your ONLY chance to correct your proof. Once published, either online or in print, no further changes can be made.

To avoid delay from overseas, please send the proof by airmail or courier.

If you have **no corrections** to make, please email | **managing editor** | to save having to return your paper proof. If corrections are light, you can also send them by email, quoting both page and line number.

• The proof is sent to you for correction of typographical errors only. Revision of the substance of the text is not permitted, unless discussed with the editor of the journal. Only **one** set of corrections are permitted.

• Please answer carefully any author queries.

• Corrections which do NOT follow journal style will not be accepted.

• A new copy of a figure must be provided if correction of anything other than a typographical error introduced by the typesetter is required.

If you do not send any corrections to the editor within 5 days, we will assume your proof is acceptable.

• If you have problems with the file please contact | **lwebb@cambridge.org** |

Please note that this pdf is for proof checking purposes only. It should not be distributed to third parties and may not represent the final published version.

Important: you must return any forms included with your proof. We cannot publish your article if you have not returned your signed copyright form.

NOTE - for further information about **Journals Production** please consult our **FAQs** at http://journals.cambridge.org/production_faqs

Author queries:

Typesetter queries:

Non-printed material:

Chapter 1: Introduction

Solar and Stellar Flares and their Impact on Planets

Kazunari Shibata

Kwasan and Hida Observatories, Kyoto University, Yamashina, Kyoto, Japan, 607-8471
email: shibata@kwasan.kyoto-u.ac.jp

Abstract. Recent observations of the Sun revealed that the solar atmosphere is full of flares and flare-like phenomena, which affect terrestrial environment and our civilization. It has been established that flares are caused by the release of magnetic energy through magnetic reconnection. Many stars show flares similar to solar flares, and such stellar flares especially in stars with fast rotation are much more energetic than solar flares. These are called superflares. The total energy of a solar flare is 10^{29} - 10^{32} erg, while that of a superflare is 10^{33} - 10^{38} erg. Recently, it was found that superflares (with 10^{34}-10^{35} erg) occur on Sun-like stars with slow rotation with frequency once in 800 - 5000 years. This suggests the possibility of superflares on the Sun. We review recent development of solar and stellar flare research, and briefly discuss possible impacts of superflares on the Earth and exoplanets.

Keywords. stars:activity, stars:flare, stars:rotation, stars:solar-type, stars:starspots

1. Introduction

The first solar flare that human beings observed was a white light flare observed by Carrington (1859) and Hodgson (1859) (Fig. 1). This flare induced the largest geomagnetic storm in the most recent 200 yr, and caused several troubles in the terrestrial civilization even in the infancy of electromagnetic technology (Loomis 1861, Tsurutani *et al.* 2003). The time between the "Carrington flare" and the geomagnetic storm was 17 hours 40 min, suggesting average propagation speed of a coronal mass ejection (CME) ejected from the flare was about 2380 km/s, which is comparable to the speed of the fastest CMEs in recent years. Hence it has been considered that the Carrington flare was one of the most energetic flares (with energy of order of 10^{32} erg) observed so far (see also reviews by Cliver and Svalgaard (2004) and Schrijver *et al.* (2012) on the Carrington-class extreme space weather event) .

After Carrington, especially since the latter half of 20th century, many solar flares have been observed in almost all electromagnetic wavelength, from radio (meter wave) to X-rays and gamma-rays (e.g., Svestka 1976, Bastian *et al.* 1998, Benz 2008, Fletcher *et al.* 2011). Typical energies of the solar flare are 10^{29}-10^{32} erg, and typical time scales are 100-10^4 sec, though there are no actual characteristic energy and time for the flare. The flare frequency statistics show that the number of flares N increases with decreasing flare energy E with a power-law distribution: $dN/dE \propto E^{-\alpha}$ and $\alpha \sim 1.6 - 2.0$ (e.g., Aschwanden *et al.* 2000). Recent observations revealed existence of microflares (10^{26}-10^{28} erg) and nanoflares (10^{23}-10^{25} erg) with a similar power-law distribution (see Fig. 12 of this paper).

The recent progress of space based solar observations in last few decades has revolutionized the solar flare research, and it has been established at least phenomenologically
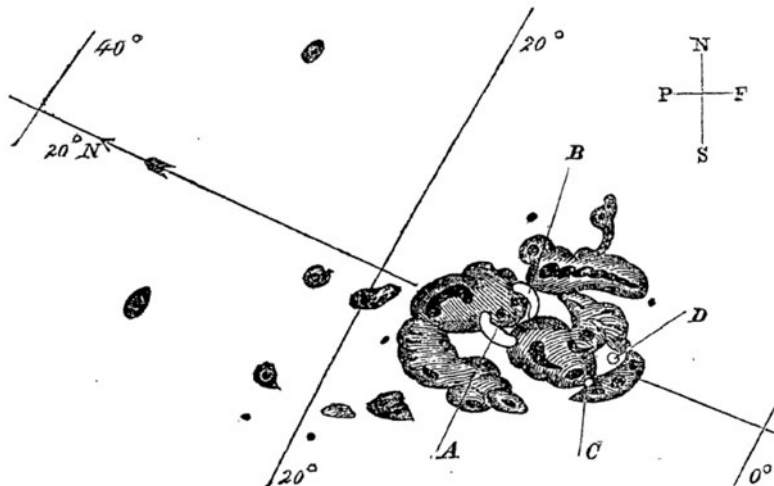
Figure 1. Sunspots and white light flare regions (A, B, C, and D) sketched by Richard Carrington (Carrington 1859).

that solar flares are caused by the release of magnetic energy stored near sunspots in the solar atmosphere through the *magnetic reconnection* (e.g., Parker 1979, Low 1996, Priest and Forbes 2000, see also Shibata and Magara 2011 for more recent review on flare MHD processes). Nevertheless, there still remains fundamental puzzles on solar flares and reconnection, such as (1) what determines the reconnection rate ? (2) how can we connect the macro-scale dynamics and micro-scale plasma physics ? (3) what is the triggering mechanism of solar flares ?

On the other hand, many stars show flares similar to solar flares in optical, radio, and X-ray wavelengths (e.g., Guedel 2002, 2004, Gershberg 2005, Benz and Guedel 2010). Sometimes the total amount of energy of a stellar flare far exceeds that of a solar flare, say, 10^{33}-10^{38} erg, especially in young stars (Koyama *et al.* 1996, Feigelson and Montmerle 1998) and binary stars, such as RS CVn (Benz and Guedel 1994). These flares are called superflares (Schaefer *et al.* 2000). Although these stellar flares have not yet been spatially resolved, there are increasing indirect evidence of reconnection mechanism similar to that for the solar flare (Shibata and Yokoyama 1999, 2002).

It has been argued that superflares would never occur on the Sun, because astronomers believed that the necessary condition for the superflare occurrence on slowly rotating Sun-like stars is the existence of hot Jupiters near to these stars (Schaefer *et al.* 2000, Rubenstein and Schaefer 2000).

More recently, many superflares (with energy of 10^{33}-10^{35} erg) were discovered in solar type stars (G-type main sequence stars) without hot Jupiters, especially in Sun-like stars whose surface temperature and rotation periods are similar to those of the Sun (Maehara *et al.* 2011, Shibayama *et al.* 2013, Notsu *et al.* 2013b). This suggests that we cannot deny the possibility of occurrence of superflares on the Sun (Shibata *et al.* 2013) .

In this article, we review the recent development of solar and stellar flare research from the view point of unified physical model based on magnetic reconnection mechanism, and briefly discuss possible impact of solar and stellar superflares on the Earth and exoplanets around these stars.
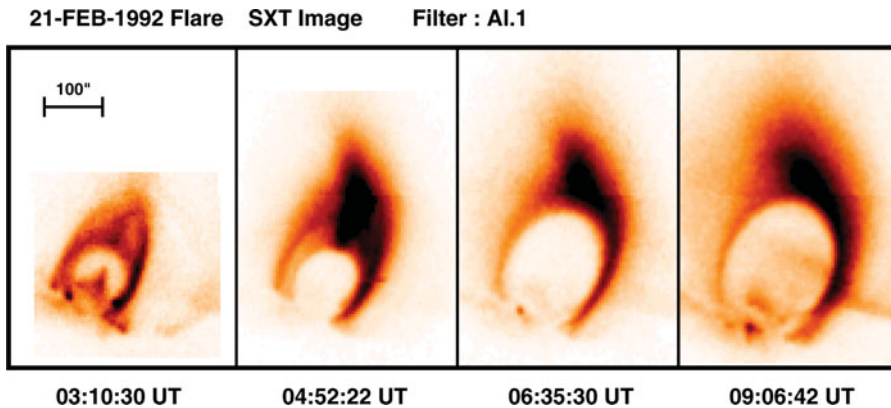
Figure 2. A soft X-ray image of an LDE (Lond Duration Event) flare with cusp shaped-loop structure, observed on Feb. 21, 1992 (Tsuneta *et al.*, 1992a; Tsuneta, 1996). Shown in reversed contrast.

2. A Unified View of Solar Flares and Flare-like Phenomena in the Solar Atmopshere

2.1. *Solar Flares, Coronal Mass Ejections, and Plasmoid Ejections*

Solar flares have been observed with Hα line from the ground based observatories, and are known to show two ribbon bright patterns in Hα images. Motivated by the observations, a standard magnetic reconnection model called *CSHKP model* (after Carmichael 1964, Sturrock 1966, Hirayama 1974, Kopp and Pneuman 1976) has been proposed. The CSHKP model predicts the formation of hot, cusp-shaped flare loops or arcades. The predicted cusp-shaped flare loops were indeed discovered by Yohkoh soft X-ray observations (Tsuneta *et al.* 1992a) (Fig. 2). Now, the standard reconnection model (CSHKP) of solar flares and flare-like phenomenon is considered established, at least, phenomenologically (Tsuneta 1996, Forbes and Acton 1996).

However, cusp-shaped flares are rather rare, and many flares do not show clear cusps. Observations show that the shape of cusp in soft X-rays is clear mainly during the *long duration event (LDE) flares*, that are long lived (more than 1 hours) flares, large in size, but have small frequency of occurrence. On the other hand, many flares (often called *impulsive flares*) are short lived, small in size, with large occurrence frequency, but show only a simple loop structure. Therefore people sometimes argued that the observed "simple loop" structure of many flares is anti-evidence of magnetic reconnection.

It was Masuda *et al.* (1994) who changed the entire scenario. He discovered the *loop top hard X-ray source* well above the simple soft X-ray loop. Since hard X-ray source is produced by high energy electrons, it provided an important evidence that a high energy process related to the central engine of flares is occurring *not* in the soft X-ray loop but above the loop. Hence even non-cusped loop flares may be energized by the magnetic reconnection high above the loop in a similar way as the reconnection in the cusp-shaped flares (Masuda *et al.* 1994). Since then, a unified model has been proposed in which the plasmoid ejection well above the loop top hard X-ray source is considered (Shibata *et al.* 1995) (Fig. 3).

Indeed, many plasmoid ejections have been discovered above the impulsive flares (Shibata *et al.* 1995, Tsuneta 1997, Ohyama and Shibata 1997, 1998, Sui *et al.* 2003, Kim *et al.* 2005, Shimizu *et al.* 2008). It is important to note that the strong acceleration of plasmoid occurs during the impulsive phase of the flares. This may provide a hint to
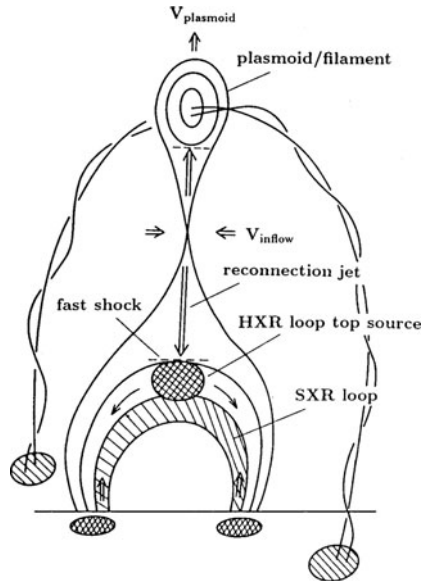
Figure 3. A unified model (*plasmoid-induced-reconnection model*) of solar flares and flare-like phenomena (Shibata *et al.* 1995), where LDE flares (Tsuneta *et al.* 1992) and impulsive flares are unified (Masuda *et al.* 1994).

understand why and how a fast reconnection occurs in actual flares (Shibata and Tanuma 2001).

About the half of the observed coronal mass ejections (CMEs; Yashiro *et al.* 2004) occur in association with flares, but the other half are not associated with flares (e.g., Munro *et al.* 1979). This also led to a lot of confusion in the community because CMEs were thought to be fundamentally different from flares (Gosling 1993). However, Yohkoh/SXT revealed the formation of *giant arcade* at the feet of CMEs (Tsuneta *et al.* 1992b, Hudson *et al.* 1995, McAllister *et al.* 1996). These giant arcades are very similar to cusp-shaped flares in morphology, but very faint in soft X-rays and Hα, and cannot be seen in non-imaging observations of soft X-rays (such as GOES) or hard X-rays. Only high-sensitive soft X-ray (and EUV) imaging observations were able to reveal the existence of giant arcade and the association of most of the non-flare CMEs with giant arcades. Hence we can now say that both flares and non-flare associated CMEs can be unified to be basically the same type of magnetically driven explosive phenomenon (Shibata *et al.* 1995, Webb and Howard 2012).

2.2. *Microflares, Nanoflares, and Jets*

Space based solar observations revealed that the solar atmosphere is full of small scale flares, called microflares, nanoflares, and even picoflares, and that these small scale flares are often associated with jets. One of the nice example of a jet is X-ray jets discovered by Yohkoh/SXT (Shibata *et al.* 1992, Shimojo *et al.* 1996). There are many pieces of observational evidence that shows that the jets are produced by magnetic reconnection (Shibata 1999). Yokoyama and Shibata (1995, 1996) performed MHD simulation of reconnection between an emerging flux and an overlying coronal field and successfully explained the observational characteristics of X-ray jets on the basis of their simulation results. A direct extension of the 2D model to 3D MHD simulation has been carried out by Isobe *et al.* (2005, 2006). They found that the onset of the Rayleigh-Taylor instability at the top of the rising emerging flux leads to formation of filamentary structures and
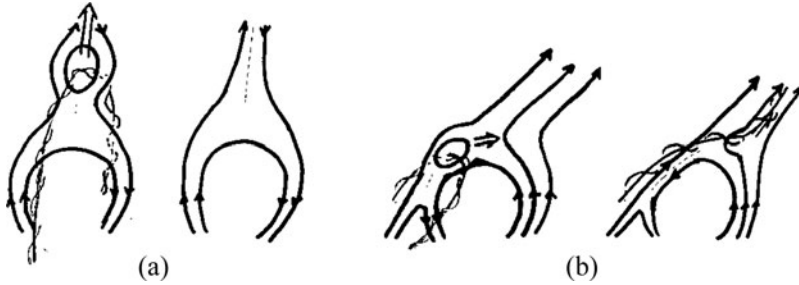
Figure 4. A unified model (*plasmoid-induced-reconnection model*) of solar flares and flare-like phenomena (Shibata 1999): (a) large scale flares (giant arcades, LDE flares, impulsive flares), (b) small scale flares (microflares, nanoflares).

patchy reconnection, in agreement with observations. As for the more recent development of 3D models, see e.g., Moreno-Insertis *et al.* (2008), Pariat *et al.*(2010), Archontis and Hood (2013).

From the high resolution images taken with Hinode/SOT, Shibata *et al.* (2007) discovered numerous, tiny *chromospheric anemone jets* (whose apparent foot-point structures are similar to "sea anemone" in a three dimensional space) in the active region chromosphere. The morphology of the chromospheric anemone jets is quite similar to that of the coronal X-ray jets (Shibata *et al.* 1992, Shimojo *et al.* 1996, Cirtain *et al.* 2007), suggesting that magnetic reconnection is occurring at the feet of these jets, although the length and velocity of these jets are much smaller than those of the coronal jets (see Takasao *et al.* 2013 for the most advanced 2D-MHD simulation model of jets based on chromospheric reconnection).

2.3. *Unified Model : Plasmoid-Induced-Reconnection Model*

Table 1 summarizes solar "flare" observations from nanoflares to giant arcades. The size and time scales range in wide values, from 200 km and 10 sec for nanoflares to 10^6 km and 2 days for giant arcades. However, it is interesting to note that if we normalize the time scale by the Alfven time (t_A), then the normalized time scale becomes similar, $100 - 300 t_A$. So the "flares" mentioned in Table 1 can be unified by a common physical process i.e. magnetic reconnection. It is quite evident that although mass ejections are common in these "flares", the morphology is quite different between the large scale and small scale flares. In large scale flares (e.g., giant arcades, LDE flares, impulsive flares), mass ejections (CMEs, filament eruptions) are bubble like or flux rope type, while in small scale flares (e.g., microflares, nanoflares), mass ejections are jets or jet-like. So what causes such morphological differences between "flares"?

Our answer to the question on morphology is as follows. According to our view (Fig. 4), the plasmoid ejection is a key process that leads to a fast reconnection (so we call "plasmoid-induced-reconnection"), since plasmoids (magnetic islands or helical flux ropes in 3D) are created naturally in the current sheets as a result of the tearing instability. In the case of large scale flares, plasmoids (flux ropes) can retain their coherent structures during the ejection even during the interaction with the ambient magnetic field. Therefore many CMEs look like the flux rope ejection. However, in the case of small scale flares, plasmoids will lose their coherent shape soon after reconnection with the ambient field, and are likely to disappear (or lose their structure) eventually after the interaction (collision) with the ambient field. As the remnant (eventually), one would expect a spinning helical jet on the reconnected field lines along with generation of Alfvén waves. We conjecture that it will explain why jets are usually observed in association with small

Table 1. Summary of Observations of Various "Flares"

"flare"	length scale (L) (10^4 km)	time scale (t) (sec)	Alfven time (t_A) (sec)	t/t_A	type of mass
nanoflares	$0.02 - 0.1$	$20 - 100$	$1 - 10$	$10 - 50$	chromospheric anemone ejection jet
microflares	$0.1 - 1$	$100 - 1000$	$1 - 10$	~ 100	coronal jet/surge
impulsive flares	$1 - 3$	$60 - 3 \times 10^3$	$10 - 30$	$60 - 100$	plasmoid/filament eruption
LDE flares	$10 - 40$	$3 \times 10^3 - 10^5$	$30 - 100$	$100 - 300$	CME/plasmoid/ filament eruption
giant arcades	$30 - 100$	$10^4 - 2 \times 10^5$	$100 - 1000$	$100 - 300$	CME/plasmoid/ filament eruption

scale flares, although this idea should be tested through future observations. It is interesting to mention that some of the observations (Kurokawa *et al.* 1987, Pike and Mason 1998, Alexander and Fletcher 1999) have revealed the formation of spinning (helical) jets after flare-like phenomena (Shibata and Uchida 1986). Further, from the Hinode/XRT observations, Shimojo *et al.* (2007) found that an X-ray loop ejection (possibly helical loop ejection) finally led to an X-ray jet. These observations support the unified model shown in Fig. 4. (See also related recent works by Filippov *et al.* (2015) and Sterling *et al.* (2015) as supporting evidence of the unified model.)

3. Plasmoid-Induced-Reconnection and Fractal Reconnection

3.1. *Plasmoid-induced reconnection*

As we have discussed in the previous section, it has become clear that the plasmoid ejections are observed quite often in solar flares and flare-like events. As the spatial and temporal resolutions of the observations have become better, more and more, smaller plasmoids have been discovered in association with flares. So, how does plasmoid ejections in flares are related with the fast reconnection?

¿From the soft and hard X-ray observations of impulsive flares, Ohyama and Shibata (1997) found that (1) a plasmoid is ejected long before the impulsive phase, (2) the plasmoid acceleration occurred during an impulsive phase (see Fig. 5(a)). As a result of the magnetic reconnection, plasmoid formation takes place (usually about 10 min) before the impulsive phase. When the fast reconnection ensues (i.e., in the impulsive phase), particle acceleration and huge amount of energy release occurs for $\sim 10 t_A$. During this process the plasmoid acceleration is closely coupled to the reconnection.

A similar relation between the energy release (and fast reconnection) and plasmoid acceleration has also been found in the case of CMEs (e.g., Zhang *et al.* 2001, Qiu *et al.* 2004) as well as in laboratory experiment (Ono *et al.* 2011). What is the physical understanding that can be drawn from the relation between the plasmoid ejection and the fast reconnection ?

Shibata and Tanuma (2001) suggested that plasmoid ejection induces a strong inflow into the reconnection region as a result of mass conservation, and drive fast reconnection. Since the inflow (that determines the reconnection rate) is induced by the plasmoid motion, the reconnection process was termed as *plasmoid-induced reconnection* (Shibata *et al.* 1995, Shibata 1999).
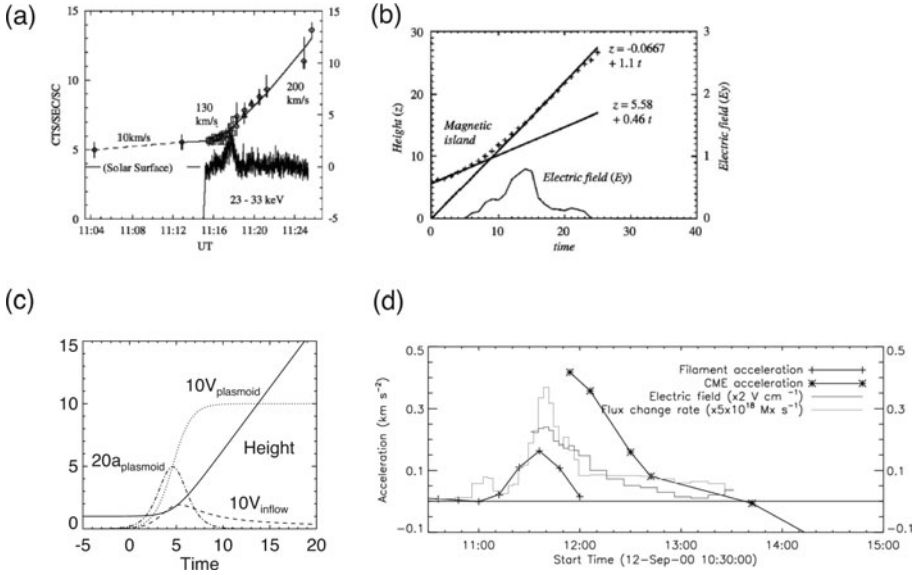
Figure 5. (a) Time variations of the height of an observed plasmoid as well as hard X-ray intensity. From Ohyama and Shibata (1997). (b) Height-time relation of a magnetic island in a two-dimensional numerical simulation, which is supposed to be the two-dimensional counterpart of a plasmoid. Time variation of the electric field (i.e., the reconnection rate $\propto V_{inflow}$) is also plotted. From Magara *et al.* (1997). (c) Analytical model of plasmoid acceleration in the plasmoid-induced-reconnection model. From Shibata and Tanuma (2001). (d) Observations of a CME and associated filament eruption (Qiu *et al.* 2004). It is seen that the filament acceleration (+) show the time variation similar to that of electric field (reconnection rate; dotted curve). From Qiu *et al.* (2004).

It should be noted that a plasmoid can be formed in any current sheet if the current sheet length is longer than the certain critical length in the tearing mode instability (Furth, Killeen, Rosenbluth 1963).

During the initial stages of plasmoid formation, a plasmoid stays in the current sheet and during this stage, the plasmoid reduces the speed of reconnection significantly by inhibiting the reconnection inflow toward the reconnection region. Only when the plasmoid is ejected out of the current sheet, a substantial amount of magnetic flux can come to the reconnection region and trigger a magnetic reconnection. This facilitates the ejection of a plasmoid via strong reconnection outflow (reconnection jet), and further in turn enables to carry new magnetic flux towards the current sheet. The positive feedback between plasmoid ejection and reconnection inflow is established, so that *fast* reconnection occurs and eventually the plasmoid is impulsively ejected out of the current sheet with the Alfvén speed.

The 2D MHD numerical simulations (Magara *et al.* 1997, Choe *et al.* 2000, Tanuma *et al.* 2001) showed such dynamics very well. Figure 5(b) shows a height-time plot from a two-dimensional MHD simulation (Magara *et al.* 1997), in which magnetic reconnection produces an ejecting magnetic island (two-dimensional counterpart of a plasmoid). The time variation of the electric field is also plotted in the height-time plot. It is found that the electric field, that is also a measure of reconnection inflow and reconnection rate, becomes large when the magnetic island (plasmoid) is accelerated.

When comparing the MHD simulation and observations, it is assumed that the time variation of electric field in the reconnection region is closely related to the time variation of hard X-ray emissions because the electric field can accelerate particles which contribute

219   to producing hard X-ray emissions. The comparison suggests that the plasmoid ejection
220   drives a fast magnetic reconnection.

    Shibata and Tanuma (2001) developed a simple analytical model for the velocity of an ejecting plasmoid by assuming (1) mass conservation between inflow and outflow $V_p W_p = V_{inflow} L_p$, and (2) the plasmoid is accelerated by the momentum added by the reconnection outflow $\rho_p L_p W_p dV_p/dt = \rho_0 V_{inlow} L_p V_A$, where V_p is the plasmoid velocity, W_p the plasmoid width, L_p the plasmoid length, V_{inflow} the inflow velocity, V_A the Alfven velocity, ρ_p the plasmoid density, ρ_0 the density of ambient plasma. ¿From these simple assumptions, they obtained the plasmoid velocity,

$$V_p = \frac{V_A \exp{(\omega t)}}{\exp{(\omega t)} - 1 + V_A/V_0}. \tag{1}$$

221 In Equation (1), ω represents the velocity growth rate of a plasmoid, defined as $\omega =$
222 $\rho_0 V_A/(\rho_p L)$.

223   The plasmoid velocity V_p, its acceleration ($a_p = dV_p/dt$), inflow velocity V_{inflow}, and
224 the height of the plasmoid obtained from the analytical model (Shibata and Tanuma
225 2001) are plotted in Figure 5(c). It is interesting to note that the acceleration and the
226 inflow velocity (or reconnection rate) derived from this simple analytical model agree
227 well with the observations (Qiu *et al.* 2004, Fig. 5(d)) as well as the numerical simulation
228 results (Cheng *et al.* 2003).

229   A detailed relation between the plasmoid velocity and the reconnection rate has been
230 investigated by performing a series of numerical experiments (Nishida *et al.* 2009). An
231 extension to 3D has also been developed by Nishida *et al.* (2013), and it was eventually
232 revealed that the formation of multiple flux ropes (helically twisted field lines) in a
233 reconnecting current sheet plays an important role in enhancing the reconnection rate.
234 These experiments show that the reconnection rate (inflow velocity) becomes larger when
235 the plasmoid is accelerated further by 3D effect (e.g., the kink instability) compared with
236 2D, whereas if the plasmoid velocity is decelerated, the reconnection rate becomes smaller.
237 When the reconnection is inhibited, the plasmoid motion (or acceleration) is stopped.

238   3.2. *Plasmoid Instability and Fractal Reconnection*

239 On the basis of nonlinear 2D MHD simulation of the magnetic reconnection on the current
240 sheet (Tanuma *et al.* 2001), Shibata and Tanuma (2001) proposed that the current sheet
241 eventually has a *fractal structure* consisting of many magnetic islands (plasmoids) with
242 different sizes (Fig. 6, see also Tajima and Shibta 1997 for an idea of fractal reconnection).

243   Once the current sheet has a fractal structure, it becomes possible to connect macro
244 scale dynamics (with flare size of 10^9 cm) and micro plasma scale dynamics (with ion
245 Larmor radius or ion skin depth of 10^2 cm). Then collisionless reconnection or anomalous
246 resistivity can be applied to flare reconnection problems (see e.g., Cassak *et al.* 2005,
247 Yamada *et al.* 2010, for the role of collisionless effects in reconnection).

248   Shibata and Tanuma (2001) presented a scenario for fast reconnection in the solar
249 corona as shown in Figure 6(b). That is, the current sheet becomes a fractal sheet con-
250 sisting of many plasmoids with different sizes. The plasmoids tend to coalesce with each
251 other (Tajima *et al.* 1987, Tajima and Shibata 1997) to form bigger plasmoids. When
252 the biggest island (i.e., monster plasmoid) is ejected out of the sheet, we have the most
253 violent energy release which may correspond to the impulsive phase of flares.

254   Solar observations show the fractal-like time variability of solar flare emission, espe-
255 cially in microwaves (Karlicky *et al.* 1996, Kliem *et al.* 2000, Barta *et al.* 2008, Aschwan-
256 den 2002), and hard X-rays (Ohki 1991). The above idea of the fractal reconnection
257 seems to explain the observations very well, since the observations suggest fragmented
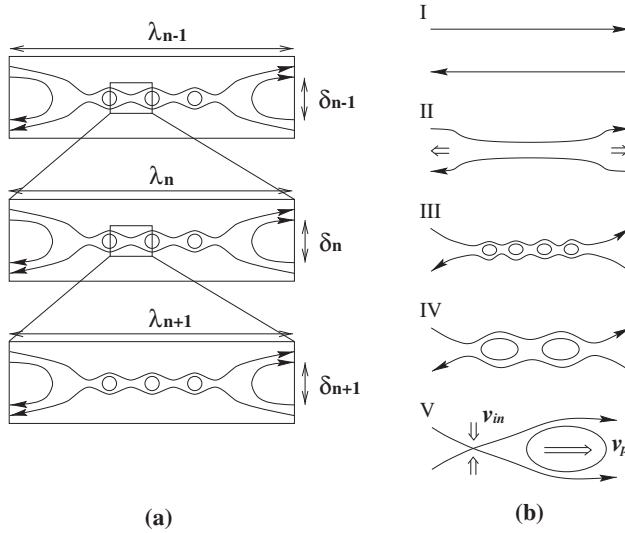
Figure 6. (a) Schematic view of the fractal reconnection. (b) A scenario for fast reconnection. I: The initial current sheet. II: The current sheet thinning in the nonlinear stage of the tearing instability or global resistive MHD instability. The current sheet thinning stops when the sheet evolves to the Sweet-Parker sheet. III: The secondary tearing in the Sweet-Parker sheet. The current sheet becomes fractal because of further secondary tearing as shown in (a). IV: The magnetic islands coalesce with each other to form bigger magnetic islands. The coalescence itself proceeds in a fractal manner. During the III and IV phases, a microscopic plasma scale (ion Larmor radius or ion inertial length) is reached, so that the fast reconnection becomes possible at small scales, V: The greatest energy release occurs when the largest plasmoid (magnetic island or flux rope) is ejected. The maximum inflow speed (V_{inflow} = reconnection rate) is determined by the velocity of the plasmoid (V_p). Hence this reconnection is termed as *plasmoid-induced-reconnection*. From Shibata and Tanuma (2001).

energy release processes in the fractal (turbulent) current sheet. For example, Karlicky *et al.* (1996) showed that the temporal power spectrum analysis of the narrow band of dm-spikes of a flare show power-law spectrum, suggesting Kolmogorov spectra after transformation of the frequency scales to the distance scales.

The tearing mode instability in Sweet-Parker current sheet is studied by Loureiro *et al.* (2007), and is now addressed as *plasmoid instability*. Numerical simulations of the nonlinear evolution of the plasmoid instability has been developed significantly in recent ten years (e.g., Bhattacharjee *et al.* 2009).

3.3. *Observational Evidence of Plasmoid-Dominated Reconnection and Fractal Reconnection*

Asai *et al.* (2004) reported that there are multiple downflow (supra arcade downflow; McKenzie and Hudson 1999, McKenzie *et al.* 2013) which are associated with hard X-ray impulsive emssions. Although the origin of supra arcade downflow is still not yet understood well, the physical relation between downflow and hard X-ray emission may be similar to the relation between plasmoid ejections and hard X-ray emissions (see Fig. 5a).

By analyzing the soft X-ray images and hard X-ray emission of a flare taken with Yohkoh satellite, Nishizuka *et al.* (2010) found multiple plasmoid ejections with velocities of 250 - 1500 km/s. They also found that each plasmoid ejection is associated with an impulsive burst of hard X-ray emssions which are a result of high energy electron acceleration and are signature of main energy release due to the fast reconnection. Later,
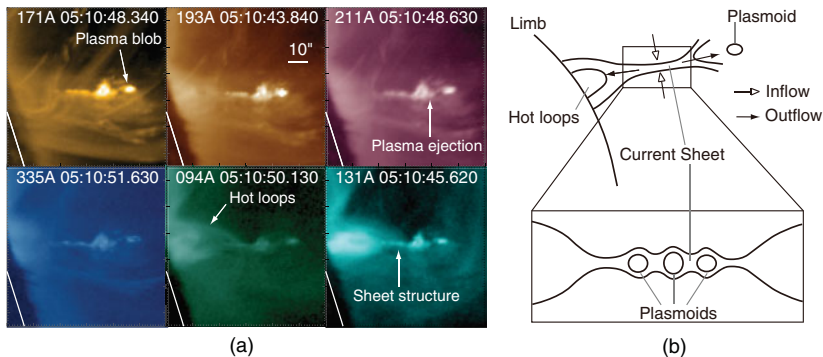
Figure 7. (a) Close-up images of the reconnection site of a solar flare in six different wavelengths (171, 193, 211, 335, 94, and 131 A) of AIA at the time when the current sheet, the plasma blob, and the hot post flare loops are observed. White solid lines indicate the solar limb. (b) Schematic diagram of the flaring region. Black solid lines indicate the magnetic field. Top: the global configuration of the magnetic field. Bottom: a close-up image of the current sheet region. From Takasao *et al.* (2012).

Nishizuka and Shibata (2013) proposed a new theoretical model of particle acceleration at the flare loop top, considering the effect of plasmoid dynamics; namely, Fermi-type acceleration occurs when a downwardly propagating plasmoid collide with the fast mode termination shock at the top of the flare loop.

Singh *et al.* (2012) analyzed chromospheric anemone jets (Shibata *et al.* 2007) observed by Hinode/SOT, and found that all the jets they analyzed show intermittent and recurrent ejections of the jet and the corresponding brightening of the loop. Such behavior is quite similar to plasmoid ejections from large flares (e.g., Nishizuka *et al.* 2010). Note that chromospheric jets are considered to be a result of *collisional* magnetic reconnection in a weakly ionized plasma (Singh *et al.* 2011). Nevertheless, the time-dependent behavior of chromospheric jets is quite similar to that of coronal reconnection (*collisionless* reconnection), suggesting the common macro-scale dynamics, i.e., plasmoid-induced reconnection in a fractal current sheet.

Takasao *et al.* (2012) observed both reconnection inflow and outflow simultaneously using SDO/AIA EUV images of a flare and derived the nondimensional reconnection rate 0.055 - 0.2. They also found that during the rise phase of the flare, some plasma blobs appeared in the sheet structure above the hot flare loops, and they were ejected bidirectionally along the sheet (see Fig. 7). This is the first imaging observations of the plasmoid-dominated current sheet in a solar flare.

3.4. *Flare Triggering Mechanism*

What is the triggering mechanism of solar flares ? This question is one of the most important questions in flare study from both scientific and application (space weather) points of view.

Chen and Shibata (2000) presented an MHD simulation model of eruptive flares and CMEs on the basis of idea from observational data analysis on the triggering of filament eruption by emerging flux (Feynman and Martin 1995). Initially, they assumed a flux rope with a filament in a stable equilibrium in 2D situation. Then, emerging flux is input from the lower boundary, which makes small scale reconnection just below the flux rope (filament). This small scale change of magnetic field configuration leads to loss of equilibrium or instability in global system, eventually leading to eruption of whole flux rope system. Kusano *et al.* (2012) extended this model to 3D successfully. It is
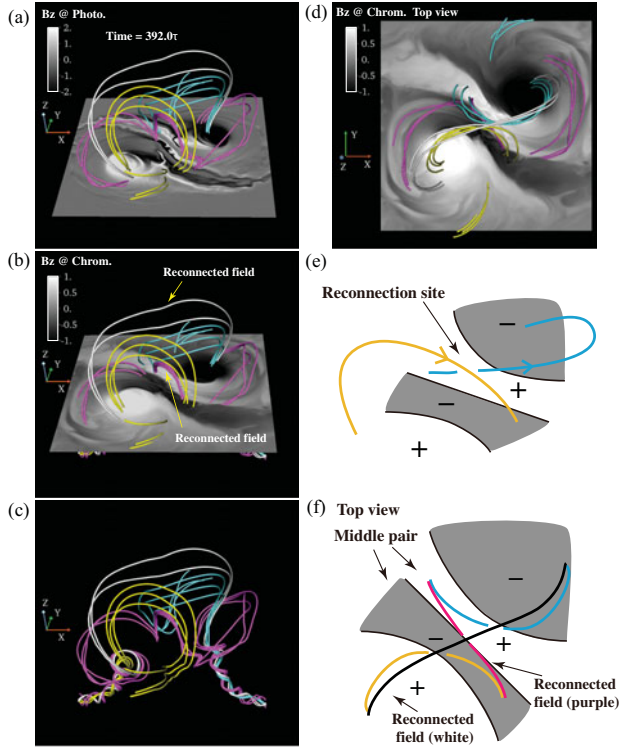
Figure 8. 3D Magnetic structure and photospheric and chromospheric line of sight magnetic fields, formed as a result of emergence of a twisted flux tube (from 3D MHD simulations by Takasao *et al.* 2015). (a)-(c): Bird's eye view. (d): Top view. (e): A schematic diagram of the merging field lines. (f): A schematic diagram of the magnetic field structure shown in the panel (d). This magnetic field configurations is very similar to those observed in the δ-type sunspot. Note also that this field line configuration shows a quadrupole magnetic field, which is favorable for occurrence of energetic flares.

also possible to trigger global eruption of the flux rope system even when emerging flux appears in a distant place from the neutral filament if the polarity distribution is favorable for local reconnection.

Here it should be stressed that reconnection is strongly coupled to eruption of the flux rope (filament or plasmoid) as discussed above. If we inhibit reconnection, the *fast* ejection of the flux rope cannot be possible. Since the flux rope becomes a CME itself or a core of CME, reconnection plays essential role in *fast* CMEs. (See Chen (2011) for a nice review on CME models and the debate on the role of reconnection in CMEs.)

In the Chen-Shibata model, small scale reconnection (cancellation) associated with emerging flux triggers large scale reconnection in the X-point high above or far from the emerging flux region. In this sense, it can be classified as *two-step reconnection* model (Wang and Shi 1993). The break out model by Antiochos *et al.* (1999) and the tether cutting model by Moore *et al.* (2001) also belong to this two-step reconnection model (see also Wang *et al.* 2002, Nagashima *et al.* 2007, Schmieder *et al.* 2013).

Shiota *et al.* (2005) compared the Chen-Shibata model with Yohkoh observations of Y-shaped ejections above giant arcades (helmet streamer), finding the signature of slow and fast mode MHD shocks associated with reconnection.

Takasao *et al.* (2015) developed the 3D-MHD simulation model of emergence of a twisted flux tube, and reproduced the basic characteristics of the δ-type sunspot, which
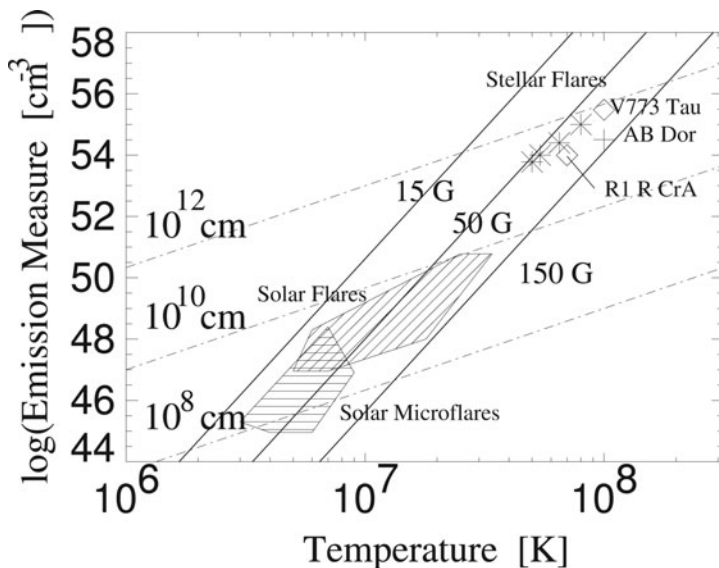
Figure 9. The EM (emission measure)−T (temperature) diagram for solar and stellar flares (Shibata and Yokoyama 2002). Hatched area shows solar flares (oblique hatch) and solar microflares (horizontal hatch), whereas other symbols denote stellar/protostellar flares. Solid lines correspond to magnetic field strength = constant, and dash-dotted lines correspond to flare size (loop length) = constant.

is one of the most important preflare signatures of energetic flares. They also revealed that during the development of the δ-type spot, the quadrupole magnetic field configuration with a current sheet was naturally formed, which is favorable for flare occurrence (Fig. 8).

4. Stellar Flares

4.1. *Unified Model of Solar and Stellar Flares: Emission Measure - Temperature Diagram*

The stellar flares show X-ray light curves similar to those of solar flares. The time scale and typical properties derived from soft X-rays also show some similarities to solar flares, though dynamic range of stellar flare parameters are much wider than those of solar flares. Recent X-ray astronomy satellite, such as ASCA, revealed that flares are frequently occurring in young stars, even in class 1 protostars (Koyama *et al.* 1996). One remarkable characteristics of these protostellar flares is that the temperature is generally high, $50 - 100$MK, much hotter than the temperature of solar flares, $10 - 20$MK. The total energy estimated is also huge, and amounts to 10^{36-37} erg, much greater than that of solar flares, 10^{29-32} erg.

Can we explain the protostellar flares by magnetic reconnection ? The answer is, of course, yes. A part of the reason of this answer comes from our finding of empirical correlation between emission measure and temperature of solar, stellar, and protostellar flares. Figure 9 shows the observed relation between emission measure and temperature of solar flares, microflares, stellar flares (Feldman *et al.* 1995), and young stellar objects (YSO) flares. It is remarkable that these data show the same tendency in a very wide dynamic range. What does this relation mean ?

Our answer is as follows (Shibata and Yokoyama 1999, 2002). Yokoyama and Shibata (1998, 2001) performed the self-consistent MHD simulation of reconnection with heat conduction and evaporation for the first time. From this simulation, they discovered a simple scaling relation for the flare temperature:

$$T \simeq 10^7 \left(\frac{B}{50\text{G}}\right)^{6/7} \left(\frac{L}{10^9\text{cm}}\right)^{2/7} \left(\frac{n_0}{10^9\text{cm}^{-3}}\right)^{-1/7} \text{K}. \tag{2}$$

This is simply a result of energy balance between reconnection heating ($B^2 V_A/4\pi$) and conduction cooling ($\kappa T^{7/2}/L$) (since the radiative cooling time is much longer than the conduction time) . With this equation and definition of emission measure ($EM = n^2 L^3$), and pressure equilibrium ($p = 2nkT = B^2/8\pi$), we finally obtain the following relation:

$$\text{EM} \simeq 10^{48} \left(\frac{B}{50\text{G}}\right)^{-5} \left(\frac{T}{10^7\text{K}}\right)^{17/2} \left(\frac{n_0}{10^9\text{cm}^{-3}}\right)^{3/2} \text{cm}^{-3}. \tag{3}$$

We plotted this relation for constant field strength (B = 15, 50, 150 G) in Figure 9. It is remarkable that these B = constant lines nicely explain empirical correlation. In other words, the comparison between observation and our theory tells that the magnetic field strength of solar and stellar flares are not so different, of order of 50-150 G. In the solar case, this value agrees well with the observations (average field strength of active region). In the case of stars, we have only limited set of observations, but these observations show a kG field in the photosphere, suggesting a 100 G average field strength in the stellar corona, consistent with our theoretical prediction.

We can also plot constant loop length lines in the diagram in Figure 9.

$$\text{EM} \simeq 10^{48} \left(\frac{L}{10^9\text{cm}}\right)^{5/3} \left(\frac{T}{10^7\text{K}}\right)^{8/3} \left(\frac{n_0}{10^9\text{cm}^{-3}}\right)^{2/3} \text{cm}^{-3}. \tag{4}$$

The loop length for microflares and flares is $10^8 - 10^{10}$ cm, consistent with the observed sizes of microflares and flares, whereas the size of stellar flare loop is huge, even larger than 10^{11} cm, comparable to or even larger than stellar radius. Because of this large size, the total energy of protostellar flares become huge and their temperature becomes hotter than those of solar flares (see eq. 2). Since it is not possible to resolve the stellar flares, the large sizes of stellar flares are simply theoretical prediction at present.

Shibata and Yokoyama (2002) noted that the EM-T diagram is similar to the Hertzsprung-Russell (HR) diagram, and examined basic properties of the EM-T diagram. They found the existence of coronal branch, forbidden regions, and also showed that flare evolution track can be plotted on the EM-T diagram, similarly to stellar evolution track in HR diagram.

4.2. *Superflares on Solar Type Stars*

By analyzing existing previous astronomical data, Schaefer *et al.* (2000) discovered 9 superflares with energy $10^{33} \sim 10^{38}$ erg in ordinary solar type stars (G type main sequence stars with slow rotation with velocity less than 10 km/s). It was argued that the cause of the superflares is the hot Jupiter orbiting near to these stars (Rubenstein and Schaefer 2000), and thus concluded that the Sun has never produced superflares, because the Sun does not have a hot Jupiter (Schaefer *et al.* 2000).

Maehara *et al.* (2012) analyzed the photometric data obtained by the Kepler space telescope (which was intended for detecting exoplanets using transit method), and found 365 superflares on 148 solar type stars. Figure 10 shows a typical example of a superflare observed by Kepler, which shows the spike-like increase (1.5 percent) in stellar brightness
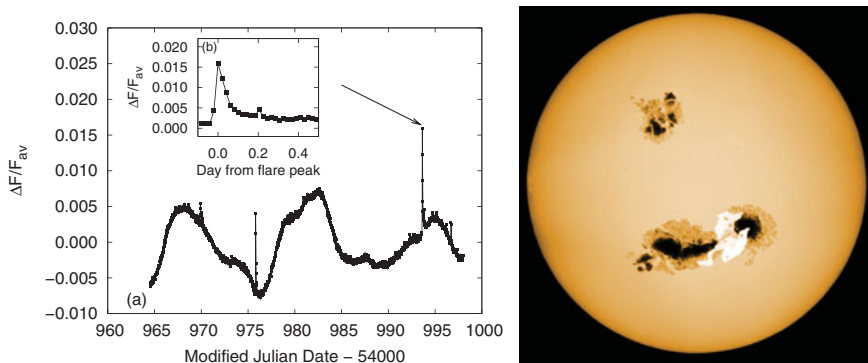
Figure 10. Left panel shows a typical example of a superflare on solar type stars (Maehara *et al.* 2012). Right panel shows artistic view of a superflare and big starspots on a solar type star on the basis of Kepler observations of superflares on solar type stars (courtesy of H. Maehara).

390 for a short time (a few hous). It should be remembered that even one of the largest solar
391 flares in recent 20 years (X18 class solar flare in 2003) showed only 0.03 percent solar
392 brightness increase for 5 to 10 minutes. The total energy of this superflare was estimated
393 to be around 10^{35} erg, 1000 times larger than the largest solar flare (10^{32} erg).
394 It is also interesting to see in Figure 10 that the stellar brightness itself shows significant
395 time variation with amplitude of a few percent with characteristic time of 10 to 15 days.
396 It is remarkable that almost all superflare stars show such a time variation of the stellar
397 brightness. Maehara *et al.* (2012) interpreted that the stellar brightness variation may
398 be caused by the rotation of a star with big starspots (Fig. 10).
399 Notsu *et al.* (2013b) developed this idea in detail using the model calculation of the
400 brightness change of the rotating star with big starspots. If this interpretation is correct,
401 we can indirectly measure the rotation period of stars and the size of star spot (or total
402 magnetic flux assuming the magnetic flux density is the same as that of the sunspot,
403 1000 to 3000 G). Since a big spot can store huge amount of magnetic energy around it, it
404 is reasonable to find that almost all superflare stars show stellar brightness change of the
405 order of a few percent or more as indirect evidence of big spots necessary for occurrence
406 of superflares.
407 According to Shibata *et al.* (2013), the maximum energy of solar flares in a spot with
408 magnetic flux density B and an area A has an upper limit determined by the total
409 magnetic energy stored in a volume $A^{3/2}$ near the spot, i.e.,

$$E_{flare} \simeq f E_{mag} \simeq f \frac{B^2}{8\pi} A^{3/2} \simeq 7 \times 10^{32} [\text{erg}] \left(\frac{f}{0.1}\right) \left(\frac{B}{10^3 \text{G}}\right)^2 \left(\frac{A}{3 \times 10^{19} \text{cm}^2}\right)^{3/2}$$

$$\simeq 7 \times 10^{32} [\text{erg}] \left(\frac{f}{0.1}\right) \left(\frac{B}{10^3 \text{G}}\right)^2 \left(\frac{A/2\pi R_{sun}^2}{0.001}\right)^{3/2} \tag{5}$$

410 where f is the fraction of magnetic energy that can be released as flare energy.
411 Figure 11 shows the empirical correlation between the solar flare energy (assuming
412 that GOES X-ray flux is in proportion to flare energy) versus sunspot area. We see that
413 the theoretical relation (upper limit is used in eq. (5)) nicely explains observed upper
414 limit of flare energy as a function of sunspot area. We also plotted the superflare data
415 on the Figure 11. It is interesting to see that there exist many superflares above the
416 theoretical upper limit. One possible solution of this apparent discrepancy is that these
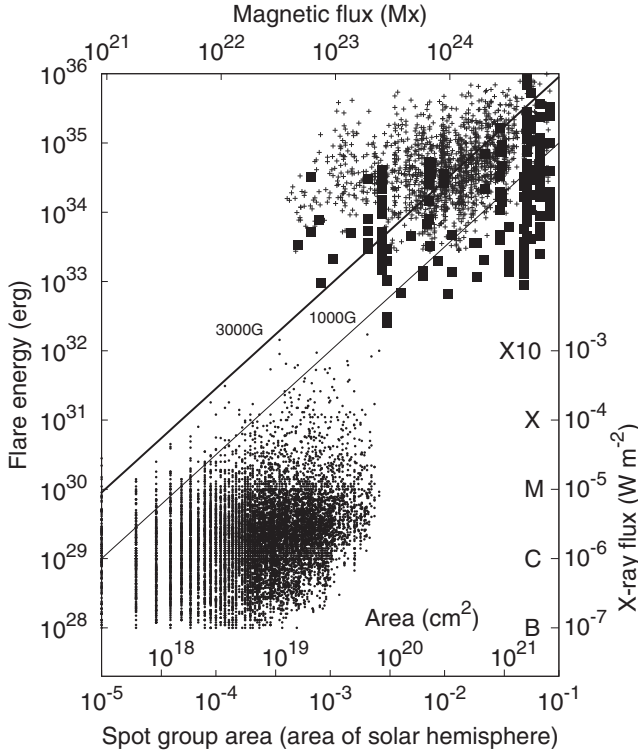417 stars (above an upper limit) may be pole-on stars. Namely, if we observe stars from the

Figure 11. Flare energy vs sunspot area (Maehara *et al.* 2015). Thick and thin solid lines in this figure represent Equation 5 for f = 0.1, B = 3, 000 and 1,000 G, respectively. Filled squares and small crosses show data of superflares on solar type stars, while small dots are solar flare data.

418 pole, we tend to estimate smaller size of starspot, because the brightness change of stars
419 (due to rotation) become small when viewed from rotating poles.
420   Later, Notsu *et al.* (2015a, b), using spectroscopic observations of 34 superflare stars,
421 confirmed the interpretation, in addition to the confirmation of the real rotation velocity
422 of these 34 stars (see also Notsu *et al.* 2013a, Nogami *et al.* 2014, Honda *et al.* 2015).
423   Figure 11 shows that both solar and stellar flares are caused by the release of magnetic
424 energy stored near spots. Figure 9 (EM-T diagram) along with Figure 11 (energy vs
425 magnetic flux diagram) makes us sure that in a statistical sense the stellar flares are
426 actually caused by the magnetic reconnection.
427   Maehara *et al.* (2015) analyzed the short time cadence data (1 min) taken by the
428 Kepler mission, and found that the duration of superflares scales with flare energy (E)
429 as $t_{flare} \propto E^{0.39}$, which is similar to the correlation between the duration of solar flares
430 and X-ray fluence E observed with the GOES ($t_{flare} \propto E^{1/3}$) (Veronig *et al.* 2002).
431 This correlation is interesting because the reconnection model of flares predict that the
432 flare energy and duration scales with the length $E \propto L^3$ and $t_{flare} \propto L$, since the flare
433 duration is basically determined by the inverse of the reconnection rate, of order of 100
434 $t_A = 100\, L/V_A$. From these relations, we find $t_{flare} \propto L \propto E^{1/3}$. This explains both solar
435 and stellar flare observations. It provides another evidence of the magnetic reconnection
436 model for *spatially unresolved* stellar flares.
        What is the frequency of solar flares and stellar superflares ? Figure 12 shows the
     occurrence frequency of flares as a function of flare energy, for solar flares, microflares,
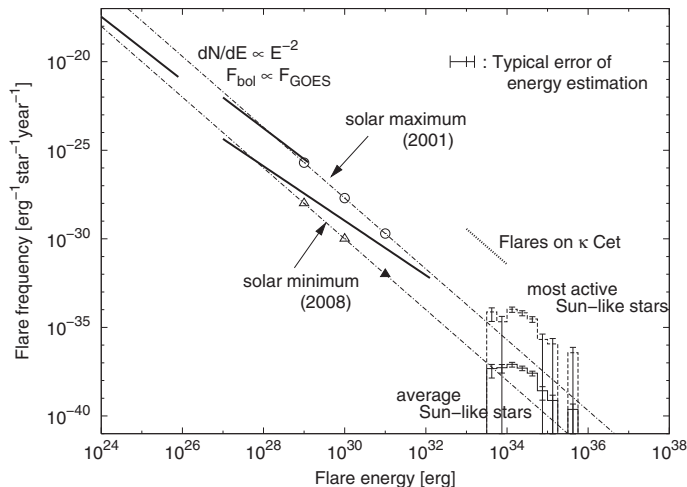
Figure 12. Occurrence frequencies of solar flares, microflares, and nanoflares. Occurrence frequency of superflares on solar type stars are also shown in this figure (Shibayama *et al.* 2013, Shibata *et al.* 2013).

nanoflares and also superflares on Sun-like stars. It is remarkable to see that superflare frequency is roughly on the same line as that for solar flares, microflares, and nanoflares,

$$dN/dE \propto E^{-2} \tag{6}$$

suggesting the same physical mechanism for both solar and stellar flares. It was found that the occurrence frequency of superflares of 10^{34} erg is once in 800 years, and that of 10^{35} erg is once in 5000 years on Sun-like stars whose surface temperature and rotation are similar to those of the Sun.

It should be noted here that there were no evidence of hot Jupiters around the superflare stars, suggesting the possibility that superflares may occur on the Sun (Nogami *et al.* 2014).

Shibayama *et al.* (2013) extended and confirmed the work by Maehara *et al.* and found 1547 superflares on 279 solar type stars from 500 days Kepler data. Shibayama *et al.* found that in some Sun-like stars the occurrence rate of superflares was very high, 4 superflares in 500 days (i.e., once in 120 days).

It is interesting to note that large cosmic ray events in 7th and 9th century are found from tree ring (Miyake *et al.* 2012, 2013). Although the source of this cosmic ray is a matter of further investigation, the possibility that such event is caused by a solar super flare cannot be ignored. The frequency of the large cosmic ray events is pretty much consistent with the superflare frequency.

What is the relation between flare energy and rotational period of stars ? Figure 13 shows the flare energy vs. the brightness variation period (interpreted as the rotation period of each star). It is remarkable that the maximum energy of stellar flares are almost independent of their rotational period, against expectation. Figure 13b also shows distribution of the occurrence frequency of flares as a function of the brightness variation period (rotational period of each star). This figure shows that as a star evolves (and its rotational period increases), the frequency of superflares decreases. Hence expected average coronal X-ray luminosity would also decrease with increasing rotational period, which agrees well with our previous observations of solar type stars. One amazing discovery from Figure 13 is that the superflare (with energy comparable to 10^{34}-10^{35} erg)
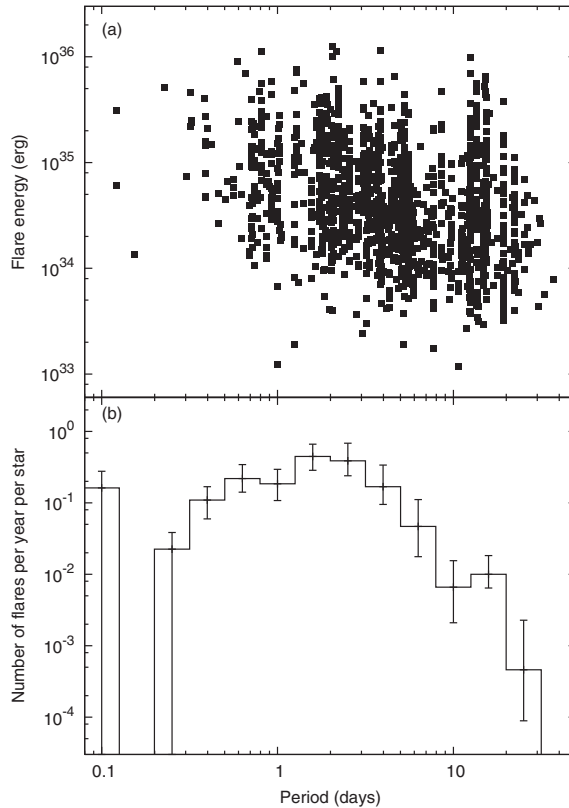
Figure 13. (a) Scatter plot of the flare energy vs. the brightness variation period (interpreted as the rotation period of each star). The period of the brightness variation in this figure was estimated by using the Kepler data. (b) Distribution of the occurrence frequency of flares as a function of the brightness variation period (rotational period of each star). The vertical axis indicates the number of flares with energy 5×10^{34} erg per star per year. The frequency distribution of superflares saturates for periods shorter than a few days. It is intereting to note that a similar saturation is observed for the relationship between the coronal X-ray activity and the rotation period of stars (Randich 2000). From Notsu, Y. *et al.* (2013b) .

463 can occur on slowly rotating stars like our Sun, even if the frequency is very low (once
464 in a few thousand years).

465   If a superflare with energy $10^{34} - 10^{35}$ erg (i.e., 100 - 1000 times larger than the largest
466 solar flares ever observed, such as the Carrington flare) occur on the present Sun, the
467 damage that such a superflare can cause to our civilization would be extremely large.
468 Hence it is very important to study the basic properties of superflares on Sun-like stars
469 to know the condition of occurrence of superflares and to understand how the superflare-
470 producing stars are similar to our Sun.

471   In this regard, Balona *et al.* (2015) examined oscillations in light curves of stellar
472 superlfares using short-cadence Kepler data, and detected flare loop oscillations similar
473 to solar flare loop oscillations (e.g., Nakariakov *et al.* 2006) in a few stars, but did not
474 find conclusive evidence as yet for flare induced global acoustic oscillations (starquakes)
475 (Kosovichev and Zharkova 1998). This kind of comparative studies between solar flares
476 and stellar superlflares will be important to reveal the difference and similarity of physical
477 conditions of our Sun and superflare stars.

It should be noted that stellar flares observed by Kepler are all "white light flares", and that the physics of solar white light flares have not yet been understood well and hence one of the hottest topics of the present flare research (e.g., Heinzel and Kleint 2014, Kowalski *et al.* 2015).

It will also be important to study the difference and similarity between solar type stars (G type dwarfs) and non-solar type stars. Candelaresi *et al.* (2013) and Balona (2015) studied superflares on non-solar type stars (i.e., A, F, K, M type stars). According to the detailed study by Maehara *et al.* (2015, in preparation), if we determine the size of spots, the maximum flare energy and frequency are uniquely determined, independent of the stellar properties (surface temperature and rotational period). (Instead, the size of spots strongly depend on the surface temperatue and rotational period.)

5. Impacts of Superflares on the Earth and Exoplanets

If a superflare with energy $10^{34} - 10^{35}$ erg would occur on the Sun or Sun-like stars, what would be expected on the environment of the Earth and exoplanets orbiting in a habitable zone around the Sun-like stars ?

It has already been discussed that if the Carrington-class flare would occur, our civilization would suffer various disasters, such as electric power outage, radio communication troubles, damages of many artificial satellites, and dangerous radiation exposure to astronauts and airline passengers (e.g., Baker 2004, Tsurutani and Lakhina 2014, Gopalswamy *et al.* 2015). Hence much more severe disasters would occur all over the world if the super-Carrington flare occur on the Sun.

What would happen on the Earth, if the super-Carrington flare occur in ancient days ? The maximum brightness (in visible light) of 10^{35} erg superflare is only a few percent larger than the average brightness of the Sun (Fig. 10), so that there is nothing changed in the terrestrial climate in a short time scale just when the superflare occurs.

However, UV and EUV would increase more than 10 percent when the superflare occurs. We can expect the average solar/stellar activity would be significantly increased (see the flare frequency of the most active Sun-like stars in Fig. 12). They affect the upper atmosphere of the Earth and exoplanets significantly.

Further, considering the empirical rule that the sunspot lifetime increases with increasing with the size of sunspot, we can expect the lifetime of large spots on superflare stars is comparable to 10 years (Shibata *et al.* 2013). Then long term climate variation may be triggered by the prolonged hyper-activity of the Sun and stars. (It is interesting to note that Saar and Brandenburg (1999) reported the existence of hyper-active phase of stellar activity cycle in some stars.) Even the enhanced visible light variation may occur as a result of the increased spot area or faculae for such a long time. (Consider what would happen if the solar brightness will be decreased by a few - 10 percent for 10 years by the effect of large spots.)

There is another effect of the superflare. That is the enhanced high energy particles by the superflare. It is not easy to estimate the radiation dose of superflare particles at the ground level but we think it is not much (less than 40 mSv). Hence we think there is no significant effect of solar energetic particles on the life on the ground in a short time scale (Takahashi *et al.* 2015, in preparation).

However, it is known that the solar energetic particles (protons) can destroy the ozone layer in the high latitude regions, since the energetic protons collide with Nitrogen to form NOx molecules, which eventually destroy ozone (O_3) moledules.

Figure 14 shows time evolution of the ozone column depth in an Earth-like exoplanet orbiting in the habitable zone around an M-type dwarf (Hawley *et al.* 1995) when a
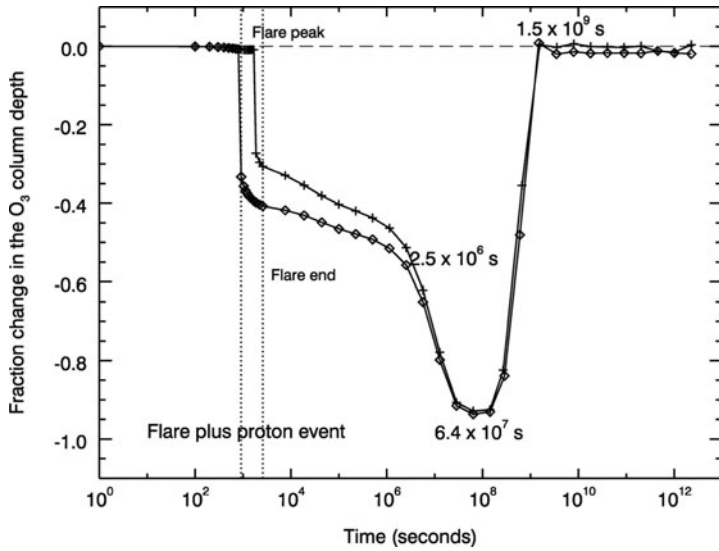
Figure 14. Time evolution of the ozone column depth compared to the initial steady state in an Earth-like exoplanet orbiting in the habitable zone around an M-type dwarf (Hawley *et al.* 1995) when a superflare occur on the M-type star. These results show the combined influence of the flare's incident UV radiation and a proton event at the peak of the flare. Line with diamonds: O_3 fraction change for a simultaneous UV and proton flux peak. Line with crosses: O_3 fraction change for a proton event with a maximum delayed by 889 s with respect to the UV flare peak. Vertical dotted lines indicate the time for the peak of the UV flare and the end of the UV flare. From Segura *et al.* (2010).

superflare occur on the M-type star (Segura *et al.* 2010). This calculation shows that the effect of the flare (protons and UV) is short (only for a few years or so), so that flares may not present a direct hazard for life on the surface of an orbiting habitable planet. Further studies will be necessary to predict the consequence and impacts of superflares on the Earth and exoplanets with various atmospheric conditions.

The study of superflares on the Sun and stars are important not only for the survivability of our society and civilization on the present and future Earth, but also for the habitability and evolution of life on exoplanets (as well as on the past Earth).

References

Alexander, D. M. & Fletcher, L. 1999, *Solar Phys.*, 190, 167
Antiochos, S. K., DeVore, C. R., & Klimchuk, J. A. 1999, *ApJ*, 510, 485
Archontis, V. & Hood, A. W. 2013, *ApJ*, 769, L21
Asai, A., Yokoyama, T., Shimojo, M., & Shibata, K. 2004, *ApJ*, 605, L77
Aschwanden, M. J., *et al.* 2000, *ApJ*, 535, 1047
Aschwanden, M. J. 2002, *Space Sci. Rev.*, 101, 1
Aulanier, G., *et al.* 2013, *A & A*, 549, 66

548 Baker, D. N. 2004, in Space Weather: The Physics Behind a Slogan, ed. K. Scherer, H. Fichtner,
549   B. Heber, & U. Mall (Lecture Notes in Physics, Vol. 656; Berlin: Springer), 3
550 Balona, L. A. 2015, *MNRAS*, 447, 2714
551 Balona, L. A., *et al.* 2015, *MNRAS*, 450, 956
552 Bárta, M., Karlický, M., & Žemlička, R. 2008, *Solar Phys.*, 253, 173
553 Bastian, T. S., Benz, A. O., & Gary, D. E. 1998, *ARAA*, 36, 131
554 Benz, A. O. 2008, *Living Reviews in Solar Physics*, 5, 1
555 Benz, A. O. & Guedel, M. 1994, *A&A*, 285, 621
556 Benz, A. O. & Guedel, M. 2010, *ARAA*, 48, 241
557 Bhattacharjee, A., *et al.* 2009, *Phys. Plasmas*, 16, 112102
558 Carrington, R. C. 1859, *MNRAS*, 20, 13
559 Carmichael, H. 1964, in Proc. of AAS-NASA Symp. on the Physics of Solar Flares, W. N. Hess
560   (ed.), NASA-SP 50, p. 451
561 Candelaresi, S., Hillier, A., Maehara, H., *et al.* 2014, *ApJ*, 792, 67
562 Cassak, P. A., Shay, M. A., & Drake, J. F. 2005, *Physical Review Letters*, 95, 235002
563 Chen, P. F. 2011, *Living Reviews in Solar Physics*, 8, 1
564 Chen, P. F. & Shibata, K. 2000, *ApJ*, 545, 524
565 Cheng, C. Z., Ren, Y., Choe, G. S., & Moon, Y.-J. 2003, *ApJ*, 596, 1341
566 Choe, G. S. & Cheng, C. Z. 2000, *ApJ*, 541, 449
567 Cirtain, J. W., *et al.* 2007, *Science*, 318, 1580
568 Cliver, E. W. & Svalgaard, L. 2004, *Solar Phys.*, 224, 407
569 Feldman, U., Laming, J. M., & Doschek, G. A. 1995, *ApJ*, 451, L79
570 Feigelson, E. D. & Montmerle, T. 1999, *ARAA*, 37, 363
571 Feynman, J. & Martin, S. F. 1995, *JGR*, 100, 3355
572 Filippov, B., *et al.* 2015, *MNRAS*, 451, 1117
573 Fletcher, L., *et al.* 2011, *Space Sci. Rev.*, 159, 19
574 Forbes, T. G. & Acton, L. W. 1996, *ApJ*, 459, 330
575 Furth, H. P., Killeen, J., & Rosenbluth, M. 1963, *Physics of Fluids*, 6, 459
576 Gershberg, R. E. 2005, Solar-Type Activity in Main-Sequence Stars (Berlin: Springer)
577 Guedel, M. 2002, *ARAA*, 40, 217
578 Guedel, M. 2004, *A&ARv*, 12, 7
579 Gosling, J. T. 1993, *JGR*, 98, 18937
580 Gopalswamy, N., Tsurutani, B. T., & Yan, Y. 2015, *PEPS*, 2, 13
581 Hawley, S. A., *et al.* 1995, *ApJ*, 453, 464
582 Heinzel, P. & Kleint, L. 2014, *ApJ*, 794, L23
583 Hirayama, T. 1974, *Sol. Phys.*, 34, 323
584 Hodgson, R. 1859, *MNRAS*, 20, 15
585 Honda, S., Notsu, Y., Maehara, H., *et al.* 2015, *PASJ*, 67, 85.
586 Hudson, H. S., & Haisch, B. and Strong, K. T., 1995, *JGR*, 100, 3473
587 Inglis, A. R., Ireland, J., & Dominique, M. 2015, *ApJ*, 798, 108
588 Isobe, H., Miyagoshi, T., Shibata, K., & Yokoyama, T. 2005, *Nature*, 434, 478
589 Isobe, H., Miyagoshi, T., Shibata, K., & Yokoyama, T. 2006, *PASJ*, 58, 423
590 Karlicky, M., Sobotka, M., & Jiricka, K. 1996, *Solar Phys.*, 168, 375
591 Kim, Y.-H., *et al.* 2005, *ApJ*, 622, 1240
592 Kliem, B., Karlicky, M., & Benz, A. O. 2000, *A& A*, 360, 715
593 Koch, D. G., Borucki, W. J., Basri, G., *et al.* 2010, *ApJ*, 713, L79
594 Kopp, R. A. & Pneuman, G. W. 1976, *Solar Phys.*, 50, 85
595 Kosovichev, A. G. & Zharkova, V. V. 1998, *Nature*, 393, 317
596 Kowalski, *et al.* 2015, *ApJ*, 798, 107
597 Koyama, K., *et al.* 1996, *PASJ*, 48, L87
598 Kurokawa, H., Hanaoka, Y., Shibata, K., & Uchida, Y. 1987, *Solar Phys.*, 79, 77
599 Kusano, K., *et al.* 2012, *ApJ*, 760, 31
600 Lin, J., Ko, Y.-K., Sui, L., *et al.* 2005, *ApJ*, 622, 1251
601 Loomis, E. 1861, *Am. J. Sci.*, 82, 318

602 Loureiro, N. F., Schekochihin, A. A., & Cowley, S. C. 2007, *Phys. Plasmas*, 14, 100703
603 Low, B. C. 1996, *Solar Phys.*, 167, 217
604 McAllister, *et al.* 1996, *JGR*, 101(A6), 13497
605 Maehara, H., Shibayama, T., Notsu, S., *et al.* 2012, *Nature*, 485, 478
606 Maehara, H., Shibayama, T., Notsu, Y., *et al.* 2015, *Earth, Planets and Space*, 67, 59
607 Magara, T., Shibata, K., & Yokoyama, T. 1997, *ApJ*, 487, 437
608 Masuda, S., Kosugi, T., Hara, T., Tsuneta, S., & Ogawara, Y. 1994, *Nature*, 371, 495
609 McKenzie, D. E. & Hudson, H. S. 1999, *ApJ*, 519, L93
610 McKenzie, D. E. 2013, *ApJ*, 766, 39
611 Miyake, F., Nagaya, K., Masuda, K., & Nakamura, T. 2012, *Nature*, 486, 240
612 Miyake, F., Masuda, K., & Nakamura, T. 2013, *Nature Com*, 4, 1748
613 Moore, R. L., Sterling, A. C., Hudson, H. S., & Lemen, J. R. 2001, *ApJ*, 552, 833
614 Munro, R. H., *et al.* 1979, *Solar Phys.*, 61, 201
615 Nagashima, K., *et al.* 2007, *ApJ*, 668, 533
616 Nakariakov, V. M., *et al.* 2006, *A&A*, 452, 343
617 Nishida, K., Shimizu, M., Shiota, D., Takasaki, H., Magara, T., & Shibata, K. 2009, *ApJ*, 690,
618   748
619 Nishida, K., Nishizuka, N., & Shibata, K. 2013, *ApJ*, 775, L39
620 Nishizuka, N., Takasaki, H., Asai, A., & Shibata, K. 2010, *ApJ*, 711, 1062
621 Nishizuka, N. & Shibata, K. 2013, *Phys. Rev. Let.*, 110, 051101
622 Nogami, D., Notsu, Y., Honda, S., *et al.* 2014, *PASJ*, 2014, 66, L4
623 Notsu, S., Honda, S., Notsu, Y., *et al.* 2013a, *PASJ*, 65, 112
624 Notsu, Y., Shibayama, T., Maehara, H., *et al.* 2013b, *ApJ*, 771, 127
625 Notsu, Y., Honda, S., Maehara, H., *et al.* 2015a, *PASJ*, 67, 32
626 Notsu, Y., Honda, S., Maehara, H., *et al.* 2015b, *PASJ*, 67, 33
627 Ohki, K. 1991, *LNP*, 387, 106
628 Ohyama, M. & Shibata, K. 1997, *PASJ*, 49, 249
629 Ohyama, M. & Shibata, K. 1998, *ApJ*, 499, 934
630 Ono, Y., *et al.* 2011, *Physics of Plasma*, 18, 11213
631 Parker, E. N. 1979, Cosmical Magnetic Fields: Their Origin and their Activity, Clarendon Press;
632   Oxford University Press, Oxford; New York
633 Pike, C. D. & Mason, H. E. 1998, *Solar Phys.*, 182, 333
634 Priest, E. R. & Forbes, T. G. 2000, Magnetic Reconnection, Cambridge University Press.
635 Qiu, Jiong, Wang, Haimin, Cheng, C. Z. & Gary, Dale E. 2004, *ApJ*, 604, 900
636 Rubenstein, E. P. & Schaefer, B. E. 2000, *ApJ*, 529, 1031
637 Schrijver, C. J. *et al.* 2012, *JGR*, 117, A08103
638 Saar, S. H. & Brandenburg, A. 1999, *ApJ*, 524, 295
639 Schaefer, B. E., King, J. R., & Deliyannis, C. P. 2000, *ApJ*, 529, 1026
640 Schmieder, B., Demoulin, P., & Aulanier, G. 2013, *AdSR*, 51, 1967
641 Segura, A., *et al.* 2010, *Astrobiology*, 10, 751
642 Shibata, K. & Uchida, Y. 1986, *Solar Phys.*, 103, 299
643 Shibata, K., Nozawa, S., & Matsumoto, R. 1992, *PASJ*, 44, 265
644 Shibata, K., *et al.* 1995, *ApJ*, 451, L83
645 Shibata, K. 1999, *Astrophys. Space Sci.*, 264, 129
646 Shibata, K. & Yokoyama, T. 1999, *ApJ*, 526, L49
647 Shibata, K. & Tanuma, S. 2001, *Earth, Planets & Space*, 53, 473
648 Shibata, K. & Yokoyama, T. 2002, *ApJ*, 577, 422
649 Shibata, K., Nakamura, T., Matsumoto, T., *et al.* 2007, *Science*, 318, 1591
650 Shibata, K. & Magara, T. 2011, Solar Flares: Magnetohydrodynamic Processes. *Linving Reviews*
651   *in Solar Physics*, 8, 6
652 Shibata, K., Isobe, H., Hillier, A., *et al.* 2013, *PASJ*, 65, 49
653 Shibayama, T., Maehara, H., Notsu, S., *et al.* 2013, *ApJS*, 209, 5
654 Shimizu, T. 1995, *PASJ*, 47, 251
655 Shimizu, M., Nishida, K., Takasaki, H., *et al.* 2008, *ApJ*, 683, L203

656   Shimojo, M., Hashimoto, S., Shibata, K., *et al.* 1996, *PASJ*, 48, 123
657   Shimojo, M., *et al.* 2007, *PASJ*, 59, S745
658   Shiota, D., *et al.* 2003, *PASJ*, 55, L35.
659   Singh, K. A. P., Shibata, K., Nishizuka, N., & Isobe, H. 2011, *Phys. Plasmas*, 18, 111210
660   Singh, K. A. P., Isobe, H., Nishizuka, N., Nishida, K., & Shibata, K. 2012, *ApJ*, 759, 33
661   Sterling, A. C., *et al.* 2015, *Nature*, 523, 437
662   Sturrock, P. A. 1966, *Nature*, 211, 695
663   Sui, L. & Holman, G. 2003, *ApJ*, 596, L251
664   Svestka, Z. 1976, Solar Flares, Springer-Verlag Berlin Heidelberg 1976
665   Takasao, S., Asai, A., Isobe, H., & Shibata, K. 2012, *ApJ*, 745, L6
666   Takasao, S., Isobe, H., & Shibata, K. 2013, *PASJ*, 65, 62
667   Takasao, S., Fan, Y., Cheung, M., & Shibata, K. 2015, *ApJ*, 813, 112
668   Tanuma, S., Yokoyama, T., Kudoh, T., & Shibata, K. 2001, *ApJ*, 551, 312
669   Tajima, T., *et al.* 1987, *ApJ*, 321, 1031
670   Tajima, T. & Shibata, K. 1997, Plasma Astrophysics, Addison-Wesley, Reading, MA
671   Tsuneta, S., *et al.* 1992a, *PASJ*, 44, L63
672   Tsuneta, S., *et al.* 1992b, *PASJ*, 44, L211
673   Tsuneta, S. 1996, *ApJ*, 456, 840
674   Tsuneta, S. 1997, *ApJ*, 483, 507
675   Tsurutani, B. T., Gonzalez, W. D., Lakhina, G. S., & Alex, S. 2003, *JGRA*, 108, 1268
676   Tsurutani, B. T. & Lakhina, G. S. 2014, *GRL*, 41, 287
677   Wang, J. & Shi, Z. 1993, *Solar Phys.*, 143, 119
678   Wang, T., *et al.* 2002, *ApJ*, 572, 580
679   Webb, D. F. & Howard, T. 2012, *Living Reviews in Solar Physics*, 9, 3
680   Yamada, M., Kulsrud, R., & Ji, H. 2010, *Rev. Mod. Phys.*, 82, 603
681   Yashiro, S., *et al.* 2004, *JGRA*, 109, 7105
682   Yokoyama, T. & Shibata, K. 1995, *Nature*, 375, 42
683   Yokoyama, T. & Shibata, K. 1996, *PASJ*, 48, 353
684   Yokoyama, T. & Shibata, K. 1998, *ApJ*, 494, L113
685   Yokoyama, T. & Shibata, K. 2001, *ApJ*, 549, 1160
686   Zhang, J., *et al.* 2001, *ApJ*, 559, 452